Title
Macromolecule Sorption and Diffusion in HEMA/MAA Hydrogels

Permalink
https://escholarship.org/uc/item/2vt6906p

Journal
Industrial & Engineering Chemistry Research, 52(50)

ISSN
0888-5885

Authors
Liu, DE
Kotsmar, C
Nguyen, F
et al.

Publication Date
2013-12-18

DOI
10.1021/ie402148u

Peer reviewed

Macromolecule Sorption and Diffusion in HEMA/MAA Hydrogels

D. E. Liu,[†] C. Kotsmar,[†] F. Nguyen,[†] T. Sells,[†] N. O. Taylor,[†] J. M. Prausnitz,[†] and C. J. Radke*,[†,‡]

[†]Department of Chemical and Biomolecular Engineering and [‡]Vision Science Group, University of California, Berkeley, Berkeley, California, 94720-1462, United States

ABSTRACT: Transient solute absorption and desorption concentration profiles were measured in a 70 wt % hydroxyethyl methacrylate (HEMA)/30 wt % methacrylic acid (MAA) anionic hydrogel using two-photon confocal microscopy. Dilute aqueous solutes included fluorescently labeled dextrans with molecular masses of 4, 10, and 20 kDa, and fluorescently labeled cationic avidin protein. Cross-linking densities with ethylene glycol dimethacrylate (EGDMA) varied from 0 to 1 wt % with polymer volume fractions increasing from 0.15 to 0.25. Average gel mesh sizes, determined from zero-frequency oscillatory shear storage moduli, ranged from about 3.6 to 8.4 nm over the cross-link ratios studied. All solutes exhibit Stokes–Einstein hydrodynamic radii obtained from measured free diffusion coefficients, D_o, comparable to or larger than the average gel mesh size. In spite of considerable size exclusion, the studied solutes penetrate the gels indicating a range of mesh sizes available for transport. Transient uptake and release concentration profiles for FITC-dextrans follow simple diffusion theory with diffusion coefficients, D, essentially independent of loading or release characteristic of reversible absorption. Although strongly size-excluded, these solutes do not interact specifically with the polymer network. Diffusivities are accordingly predicted from a large-pore effective-medium (LPEM) model developed to account for solute size, hydrodynamic drag, and distribution of mesh sizes available for transport in the polymer network. For this class of solute, and using no adjustable parameters, diffusivities predicted from the new effective-medium model demonstrate good agreement with experiment. For the specific-interacting cationic protein, avidin, gel loading is 3 orders of magnitude slower than that of dextran of similar hydrodynamic radius. Desorption of avidin is not complete even after 2 weeks of extraction. On the basis of size alone, avidin is strongly size-excluded, yet it exhibits a partition coefficient of over 20. For the positively charged protein, we observed specific ion binding on the negatively charged carboxylate groups of MAA-decorated polymer strands in the larger mesh spaces. Simple linear sorption kinetics gives an adsorption time constant of 5 min and a desorption time constant of about 20 days, suggesting nearly irreversible uptake of cationic avidin on the anionic gel matrix.

1. INTRODUCTION

Diffusion of solute molecules in hydrogels is of interest in a wide variety of applications including chromatographic separations,[1–4] membrane separation,[1,5] and encapsulation of cells in hydrogels for biomedical treatment.[6–8] Due to their biocompatibility, hydrogels are extensively used in pharmaceutics for delivery of bioactive agents,[5,9,10] and for synthesis of artificial organs.[5,11] Soft contact lenses are hydrogels[12–14] and can be used to deliver drugs[15–19] and comfort/wetting agents to the eye.[20,21]

Hydrogels are cross-linked hydrophilic polymers swollen in aqueous media.[5,22–24] Cross-links between chains are formed by physical entanglements, such as van der Waals attraction, hydrogen bonding, ion binding, or, most commonly, covalent bonds. The three-dimensional structure of a gel is best described by a mesh whose spaces between polymer chains are filled with aqueous solution. Mesh size, ξ, gauges the distance between cross-links in the polymer network.[25] Hydrogels are especially appealing for solute delivery because their mesh sizes can be controlled, for example, by altering temperature[10] or pH.[11]

Solute diffusion in hydrogels occurs primarily through the water fraction. Diffusivities of aqueous solutes in hydrogels are diminished relative to their bulk values by interaction with the polymer chains including hydrodynamic drag, physical obstruction, electroosmosis, and specific binding.[26–29] The cross-linking process during hydrogel synthesis produces a distribution of polymer-strand molecular weights between cross-links and, correspondingly, a distribution of mesh sizes.[9,30] Thus, in addition to solute-chain interactions, significant size exclusion can occur when solute size is comparable to gel mesh size.[31]

Because of extensive application, a large effort has been expended on studying solute diffusion in hydrogels both experimentally and theoretically.[2–4,9,17,26–29,32–57] Published work falls into two classes: diffusion of small solutes, such as salts and small sugars, and diffusion of larger solutes, such as polymers, surfactants, and proteins whose sizes are comparable to the mesh size. Most studies are in the first class using a Stokes cell or back extraction; concentration profiles are not available. In most all cases, the hydrogels exhibit relatively large water contents (more than 90%), and accordingly, solute size exclusion is not extreme.

Little attention has been given to diffusion of charged macromolecules in ionic hydrogels of opposite charge. Several investigators have established that oppositely charged macromolecules are adsorbed in ionic hydrogels, especially at low ionic strengths.[1–4] Large counterion solutes provide an opportunity to study the transport rates of solutes that

experience both size exclusion and adsorption to the polymer network.

This work considers application of hydrogels to soft contact lenses,[31] characterized by relatively low water content[46] and, accordingly, small mesh sizes. Conversely, aqueous solutes of interest, including surfactants, polymers, and proteins,[12,13,20,21] are comparably large. Thus, we study diffusion of solutes in a representative soft-contact-lens material with relatively high polymer content where solute and mesh sizes are similar. Two-photon confocal microscopy detects transient fluorescence-intensity profiles within the gel. All diffusivity measurements are performed in sufficient aqueous indifferent electrolyte that electrostatic fields are absent.

Sorption of fluorescently labeled dextrans and fluorescently labeled avidin is investigated in both loading and release directions. The anionic hydrogels consist of 70 wt % hydroxyethyl methacrylate (HEMA)/30 wt % methacrylic acid (MAA) in aqueous phosphate buffer (PBS, pH 7.4, ionic strength = 0.15 M) with cross-link densities ranging from 0 to 1 wt %. Average gel mesh size is determined from oscillatory shear rheometry and Gaussian-chain elastic-rubber theory.[31] Solute sizes are determined from independent measurement of the bulk aqueous diffusion coefficient in a restricted diffusion cell[58,59] and Stokes−Einstein theory.[60] Significant size exclusion is evident with equilibrium solute partition coefficients as low as 0.001 for the largest dextran molecule. To understand nonspecific-interacting dextran diffusivities in the gel, we interpret experimental data using an extended effective-medium theory with all parameters determined independently. For positively charged avidin fluorescein conjugate (Fl-avidin), however, uptake and release rates are controlled by specific electrostatic adsorption onto the negatively charged polymer chains. Accordingly, avidin concentration profiles in the gel are determined by both diffusion and adsorption kinetics.

2. EXPERIMENTAL SECTION

2.1. Gel Synthesis and Characterization. Hydrogels of 70 wt % HEMA (No. 128635, Sigma Aldrich, St. Louis, MO, USA)/30 wt % MAA (No. 155721, Sigma Aldrich, St. Louis, MO, USA) were synthesized by simultaneous copolymerization and cross-linking of monomers with ethylene glycol dimethacrylate (EGDMA; 335681, Sigma Aldrich, St. Louis, MO, USA) as the cross-linking agent at 0−1 wt % in aqueous solution.[22,61] Details are described elsewhere.[31] Once synthesized between shimmed glass plates, 6 mm × 6 mm films were cut and placed into scintillation vials filled with phosphate buffer solution (PBS: 0.15 M NaCl, 0.017 M Na$_2$HPO$_4$·7H$_2$O, and 0.003 MNaH$_2$PO$_4$·H$_2$O; pH 7.4) for no less than 7 days to allow complete swelling. Because the pK_A of monomeric MAA is 5.5, the synthesized gels are anionic. The Debye length of the background PBS electrolyte is about 0.5 nm, so polymer matrix charge is effectively screened. Consequently, nonspecific electrostatic-field effects on solute diffusion fluxes are absent. All experiments were performed at ambient temperature.

Equilibrium swollen gels of varying cross-linked densities were characterized by their water content from thermal gravimetric analysis (TGA; Model 2950, TA Instruments, New Castle, DE, USA) and by their average mesh size obtained from linear oscillatory rheometry (Physica MCR301 Rheometer, Anton-Paar, Ashland, VA, USA).[31]

Following Peppas et al.,[22] the measured zero-frequency shear storage modulus, $G'(0)$, for each cross-link density swollen gel was converted to an average mesh size as

$\langle \xi \rangle = l_{c-c}\{2C_n\rho_2RT/[M_rG'(0)]\}^{1/2}\varphi^{-1/6}$, where l_{c-c} is the length of a covalent carbon−carbon bond in the backbone (0.154 nm) and C_n is the Flory characteristic ratio or rigidity factor.[62,63] For HEMA/MAA gels, C_n equals 6.9.[22] M_r is the molecular weight of a repeat unit, 112.7 g/mol for the 70 wt % HEMA/30 wt % MAA copolymer, and ρ_2 is the density of the dry polymer (1070 kg/m^3 for 70 wt % HEMA/30 wt % MAA). Table 1 reports the calculated average mesh sizes, $\langle \xi \rangle$, for gels

Table 1. Hydrogel Polymer Volume Fraction and Average Mesh Size

cross-link density (wt % EGDMA)	φ^a	$\langle\xi\rangle^b$ [nm]
0	0.143	8.3
0.01	0.15	7.9
0.025	0.148	8.3
0.05	0.143	8.3
0.1	0.154	7.7
0.25	0.165	7.3
0.5	0.183	6.3
0.75	0.2	5.0
1	0.227	3.6

^{a}Measured with TGA. ^{b}Calculated following Peppas et al.[22]

with different cross-link densities and corresponding polymer volume fractions, φ.[31] Average mesh size increases from 3.6 to 8.3 nm for increasing water volume fractions from 0.74 to 0.86. An extended Ogston mesh-size distribution[30] adequately fits the data in Table 1, giving an approximate polymer-strand radius a_f = 2 nm (see Figure 8 of Kotsmar et al.[31]).

2.2. Solute Characterization. Fluorescein isothiocyanate dextrans (FITC-dextran4, MW = 4000 g/mol; FITC-dextran10, MW = 10 000 g/mol; FITC-dextran20, MW = 20 000 g/mol) were obtained from TdBCons (Uppsala, Sweden). They were extensively dialyzed prior to experiment to remove any free label. Each FITC-dextran solution was placed in a Slide-A-Lyzer Dialysis Cassette (No. 66212, 2000 molecular weight cutoff, Thermo Scientific) for 1 h at room temperature followed by 1 week in a commercial refrigerator with the surrounding PBS dialyzing solution changed daily. Only FITC-dextran20 showed a decrease in gel diffusivity compared to those of the supplied materials. Avidin fluorescein conjugate (Fl-avidin, No. A821) was obtained from Invitrogen (Eugene, OR, USA) and was used as received.

To ascertain the hydrodynamic radii of the chosen solutes, we determined bulk diffusion coefficients in a restricted diffusion cell[58] using UV/vis absorption.[59] The experimental protocol is described by Kotsmar et al.[31] From the measured diffusion coefficient, the hydrodynamic radius of the aqueous solute was ascertained from the Stokes−Einstein relation.[44,52,60] Our measured bulk diffusivities show good agreement with literature values.[31,56] Table 2 displays the hydrodynamic diameters, $2a_S$, of fluorescently labeled dextrans and avidin. Reported diameters suggest that aqueous Fl-avidin is more

Table 2. Solute Hydrodynamic Diameters

solute	MW [g/mol]	$2a_S$ [nm]
FITC-dextran4	4 000	3.1[56]
FITC-dextran10	10 000	4.7[56]
FITC-dextran20	20 000	6.7[56]
Fl-avidin	68 000	7.05[31]

compact compared to the corresponding branched linear polymers of smaller or comparable molecular weight. Comparison of Tables 1 and 2 reveals that all solutes are comparable to or larger than the average gel mesh sizes. Nevertheless, all solutes penetrate the gels but with small partition coefficients as low as 0.001 due to significant size exclusion.[31]

2.3. Gel−Solute Confocal Microscopy. Diffusion coefficients of the fluorescently labeled solutes in the hydrogels were determined using two-photon confocal microscopy.[64−67] A distinct advantage of two-photon fluorescence is excitation in a small volume ($\sim$1 μm^3) allowing minimal photobleaching and permitting transient-profile assessment. At dilute solute concentrations between 10^{-5} and 5×10^{-4} M, fluorescence intensity measured both in solution and in the gel was confirmed linearly proportional to the dye concentration.[68] Because concentrations are measured in the gel phase, diffusion coefficients are directly ascertained with no need for correction by a partition coefficient. We obtained both loading and unloading profiles to ascertain reversibility of solute uptake and release. A Carl Zeiss (Jena, Germany) 510 LSM META NLO AxioImager Confocal Microscope equipped with a Spectra-Physics (Santa Clara, CA) MaiTai HP DeepSee Laser was used for two-photon imaging at 780 nm. Fluorescence emission was collected with a Plan-Neofluar 10x/0.30 NA objective (Carl Zeiss GmbH) using a 500−550-nm emission filter.

For solute-absorption measurements, 6 mm × 6 mm, 800−2500-μm-thick swollen gel sheets were first soaked in the chosen aqueous-PBS/solute solution under magnetic stirring at 400 rpm. At selected times, a gel sheet was removed from solution, lightly blotted on both faces, placed flat on a microscope slide (VWR Micro Slides, 48300-047, VWR International, West Chester, PA, USA), and covered with a microscope cover glass (No. 12-541-B, Fisher Scientific, Fair Lawn, NJ, USA) to prevent water evaporation. Vertical scanning on the microscope was performed downward through the gel at 3-μm intervals over the entire slab thickness at an instrument-set scan rate of about 10 μm/s. To minimize edge effects, scans were performed in the middle of the gel slab. Figure 1a shows typical two-photon confocal fluorescence micrographs of FITC-dextran20 absorbing into a 70 wt % HEMA/30 wt % MAA hydrogel slab with 0.25 wt % cross-link density ($\langle\xi\rangle$ = 7.3 nm) at increasing exposure times. FITC-dextran20 permeates the gel from both faces in the expected fashion for diffusive transport. Longer exposure times give more penetration toward the slab center with surface intensities remaining nearly constant. Complete equilibration occurs in less than 1 day for this particular solute/gel combination.

For solute-desorption measurements, nascent swollen gel sheets were first soaked in the pertinent aqueous-solute solution under magnetic stirring for at least 48 h at 400 rpm to guarantee complete saturation. Sample scans confirmed that all solutes, except avidin, reached a uniform-equilibrated concentration profile.[31] Measured water contents of solute-loaded and nascent swollen gels were identical. Accordingly, for the dilute solutes employed, solute loading does not alter overall swelling. After equilibration, solute-saturated gel sheets were placed in a large volume of solute-free PBS solution also under magnetic stirring at 400 rpm. At selected release times, a gel sheet was scanned similarly to the absorption measurements, but without blotting. Figure 1b shows sample fluorescence micrographs of FITC-dextran20 desorption from a 70 wt % HEMA/30 wt % MAA hydrogel with 0.25 wt %
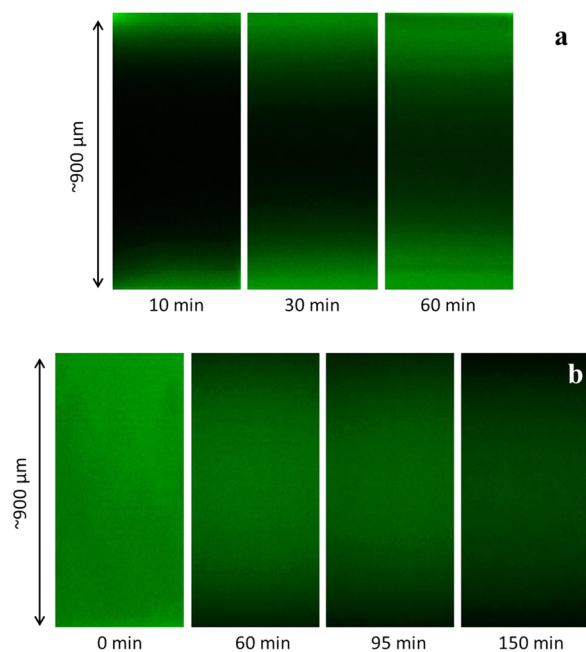

Figure 1. (a) Fluorescence micrographs of FITC-dextran20 absorption into a 70 wt % HEMA/30 wt % MAA hydrogel with 0.25 wt % cross-link density at different absorption times. (b) Fluorescence micrographs of FITC-dextran20 desorption from a 70 wt % HEMA/30 wt % MAA hydrogel with 0.25 wt % cross-link density at different desorption times.

cross-link density ($\langle\xi\rangle$ = 7.3 nm). As desorption progresses, fluorescence intensity decreases from the center toward the two surfaces of the gel slab (i.e., top and bottom of the micrographs in Figure 1, respectively) as solute diffuses out from the gel and into the surrounding excess PBS solution. After sufficient time, total desorption from the gel is observed, although complete release can take many days depending on the particular solute molecule and gel under study.

As illustrated in Figure 2, images obtained from two-photon confocal microscopy were converted into fluorescence intensity versus position profiles. Because fluorescence intensity varies linearly with dye concentration, solute intensity profiles are equivalent to transient concentration profiles in the gel. Typically, four to six different scanned intensity profiles of each micrograph were averaged into one profile. Resulting averaged intensities were then smoothed with the 10 most nearby points by an adjacent-averaging smoothing technique.[69] Background fluorescence intensity was then subtracted.

Figure 2a gives loading intensity profiles corresponding directly to the micrographs in Figure 1a, while Figure 2b reflects release intensity profiles corresponding directly to micrographs in Figure 1b. The distance scale is from top to bottom of the gel sample. Characteristic diffusion-profile shapes are found for each sorption direction. Because of signal attenuation, intensity profiles are not strictly symmetric with intensities near the bottom of the gel slab slightly lower than those near the top of the slab. This effect is clearly seen in the fully saturated or zero-time profile in Figure 2b. Detected fluorescence intensities decline when a thick sample is scanned deeply. Higher solute concentrations are more prone to this decline. To overcome the lack of uniform signal detection at the solute concentrations studied, we evaluated data measured only in the top half of the gel where intensities are practically
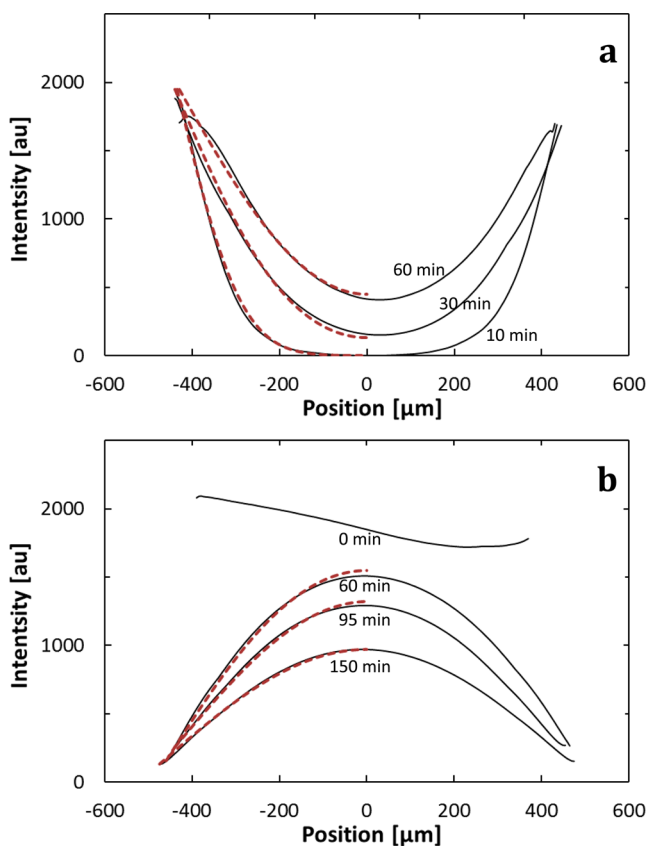
Figure 2. (a) Transient intensity profiles of FITC-dextran20 absorption into a 70 wt % HEMA/30 wt % MAA hydrogel with 0.25 wt % cross-link density. (b) Transient intensity profiles of FITC-dextran20 desorption from a 70 wt % HEMA/30 wt % MAA hydrogel with 0.25 wt % cross-link density. Solid and dashed lines represent measured profiles and best fits to eqs 2–4, respectively.

independent of sample depth. For our gel samples, signal attenuation in the top half of the gel is minimal and does not infect solute diffusivities.

A second artifact arises in the experimental intensity data directly at the top surface of the gel, best illustrated by close examination of the absorption profiles in Figure 2a. Solute concentrations at the top surface should be large and remain at a single large value during loading. In some cases, however, the maximum fluorescence intensity measured in the gel sample is not exactly at the top surface of the gel, but sometimes is observed downward to a depth of 50 μm. Most likely, the gel surface is locally dried due to the blotting procedure. Consequently, we do not directly use the measured surface intensities in the fitting procedure to obtain solute/gel diffusion coefficients. We find that stirring the surrounding bulk aqueous phase at higher speeds, or even no stirring, has no influence on the measured concentration profiles, confirming negligible external mass-transfer resistance.

2.4. Nonadsorbing-Solute–Gel Diffusion Coefficients. At dilute concentration, solute diffusion in a nonadsorbing gel follows Fick's second law with a constant diffusion coefficient

$$\frac{\partial C(t, x)}{\partial t} = D \frac{\partial^2 C(t, x)}{\partial x^2} \tag{1}$$

where C is the solute concentration per unit volume of liquid, t denotes time, D is the solute diffusivity in the gel, and x is the spatial coordinate for a domain thickness $2L$ with $x = 0$ locating

the center of the gel slab. As highlighted above, only data for $-L < x < 0$ were analyzed. For both loading and release, symmetry is demanded at the centerline. For loading, $C(t,-L) = C_\infty$, where C_∞ is the final solute concentration in the gel in equilibrium with the bulk aqueous solute solution. For release, $C(t,-L) = 0$ since the desaturating aqueous solution is devoid of solute and in excess. Initial conditions are $C(0,x) = 0$ for adsorption and $C(0,x) = C_\infty$ for desorption because desaturation occurs from the initial equilibrium state.

Let $A_n(t,x;t^*)$ be defined as

$$A_n(t, x; t^*) \equiv 2\frac{(-1)^n}{\lambda_n}\{1 - \exp[-\lambda_n^2 Dt^*/L^2]\}$$

$$\times \exp[-\lambda_n^2 Dt/L^2]\cos[\lambda_n x/L] \tag{2}$$

where $\lambda_n \equiv (2n + 1)\pi/2$ and t^* is a final loading time. Absorption then follows according to

$$\frac{C(t, x)}{C_\infty} = 1 - \sum_{n=0}^{\infty} A_n(t, x; \infty) \tag{3}$$

and desorption from an equilibrated gel at C_∞ obeys the relation

$$\frac{C(t, x)}{C_\infty} = \sum_{n=0}^{\infty} A_n(t, x; \infty) \tag{4}$$

Transient intensity profiles are fit to eqs 2–4 by Levenberg–Marquardt least-squares-error minimization[70] to obtain separate diffusion coefficients in the absorption and desorption directions. We use 100 terms in the summations.

For loading profiles, we do not rely on the measured surface intensity at $x = -L$ because of surface blotting. To obtain C_∞, we use an extrapolated concentration from least-squares fitting of the concentration profile and average over all measured profiles in that loading run. All profiles are then adjusted to this average surface concentration and re-fit for the best diffusion coefficient by a second least-squares minimization. For any given solute–gel system, no less than four data sets at different absorption times were fit to find the diffusion coefficient. Resulting diffusion coefficients were then averaged by linearly weighting them by the inverse mean-square error of a particular profile. Likewise, the overall standard deviation of the diffusion coefficient was established by similar linear weighting of the standard deviations for each transient profile.

For the corresponding solute-desorption experiments, initial fluorescence intensity of the dye-saturated gel for each solute–gel system was measured and set as constant and proportional to C_∞. Thereafter, local equilibrium with the excess solute-free aqueous solution established the gel surface concentration: $C(t,-L) = 0$. Figure 2b, however, illustrates that solute fluorescence at the surface, although small, is not exactly zero after background subtraction. Because this concentration was always less than 5% of the saturated concentration, it was averaged over the measured profiles and subtracted from the measured intensity profiles. Best fitting of the diffusion coefficient and assessment of standard deviation from the desorption profiles was then performed as for the absorption profiles.

3. RESULTS

3.1. Nonspecific-Interacting Solutes. Table 3 summarizes diffusion coefficients for absorption measured for the three

Table 3. Solute–Hydrogel Absorption Diffusivities

φ	$D \times 10^7$ [cm²/s]		
	FITC-dextran4	FITC-dextran10	FITC-dextran20
0.143 (0)[a]	4.44 ± 0.84	2.52 ± 0.94	0.982 ± 0.13
0.154 (0.10)	3.15 ± 0.20	1.64 ± 0.63	0.669 ± 0.17
0.165 (0.25)	2.11 ± 0.086	1.10 ± 0.15	0.675 ± 0.25
0.183 (0.50)	1.16 ± 0.04	0.549 ± 0.079	0.737 ± 0.053
0.227 (1.0)	1.22 ± 0.18	0.689 ± 0.117	0.404 ± 0.12

[a]Numbers in parentheses correspond to wt % cross-linking density.

labeled dextrans in five different polymer-content 70 wt % HEMA/30 wt % MAA gels at pH 7.4. In spite of molecular hydrodynamic sizes comparable to or larger than the average gel mesh size, all solutes permeate all gels. As expected, diffusivities of the same solute decrease with increasing polymer content (i.e., with decreasing mesh size). In the same cross-link-density gel, solute uptake rates decrease with increasing molecular weight, also as expected.

Table 4 reports the corresponding solute–gel diffusion coefficients for desorption from the same cross-link-density

Table 4. Solute–Hydrogel Desorption Diffusivities

φ	$D \times 10^7$ [cm²/s]		
	FITC-dextran4	FITC-dextran10	FITC-dextran20
0.143 (0)[a]	2.61 ± 0.97	1.25 ± 0.46	0.777 ± 0.063
0.154 (0.1)	2.34 ± 0.47	–	0.809 ± 0.11
0.165 (0.25)	1.84 ± 0.07	1.45 ± 0.20	0.787 ± 0.059
0.183 (0.5)	1.56 ± 0.29	0.63 ± 0.36	0.897 ± 0.15
0.227 (1.0)	1.03 ± 0.07	0.54 ± 0.11	0.617 ± 0.063

[a]Numbers in parentheses correspond to wt % cross-linking density.

hydrogels as those for absorption. Trends are identical to those for the loading direction. Comparison of the loading and release diffusion coefficients reveals agreement, although the solute-desorption diffusivities are somewhat smaller than those for absorption. Lack of significant difference between absorption and desorption diffusion coefficients suggests that the solute molecules do not interact strongly with the gel matrix. Loading and release are reversible. Indeed, we find that all dextran solutes are completely extracted from the HEMA/MAA gels to within experimental precision. Concomitantly, all solutes are size-excluded from a large portion of the liquid void space in the gels.[31] The somewhat smaller desorption diffusion coefficients might be attributed to small interaction with the polymer strands in the larger mesh-size spaces.

Figure 3 summarizes the loading (closed symbols) and release (open symbols) diffusivities, D, in the 70 wt % HEMA/30 wt % MAA gels from Tables 3 and 4 normalized by their corresponding bulk diffusivities, D_o, as a function of polymer volume fraction, φ, for the three labeled dextrans. For comparison, relative macromolecular diffusivities measured in agarose[36] and polyacrylamide[37] gels are shown. Clearly, our dextran–HEMA/MAA data correspond to higher-polymer-content gels where size exclusion is pronounced. Our data fall in line with those measured by fluorescence recovery after photobleaching (FRAP) by Johnson et al.[36] for proteins in agarose gels, but are somewhat larger than those by Tong and Anderson[37] in polyacrylamide gels. FRAP does not distinguish between diffusion in the uptake and release modes.
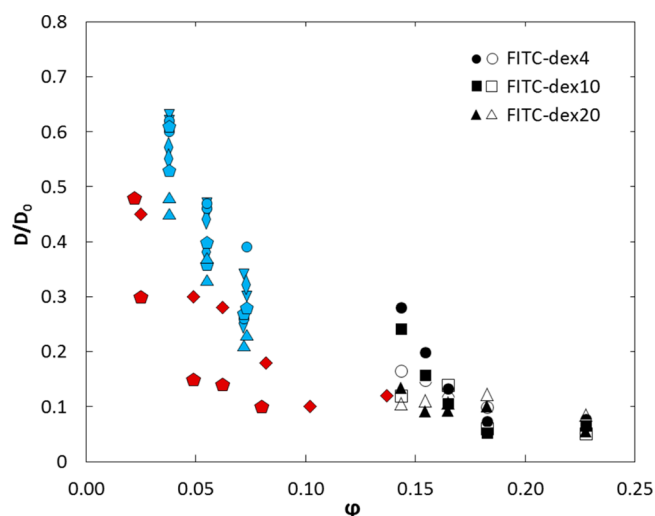

Figure 3. Relative diffusion coefficients of FITC-dextran4 (●, ○), FITC-dextran10 (■, □), and FITC-dextran20 (▲, △) in 70 wt % HEMA/30 wt % MAA hydrogels as a function of polymer volume fraction. Filled symbols correspond to the loading direction, while open symbols correspond to the release direction. Also shown are the relative macromolecular diffusion coefficients of lactalbumin (blue downward triangles), ovalbumin (blue diamonds), bovine serum albumin (blue pentagons), and Ficolls of molecular weights 21 kDa (blue circles) and 61 kDa (blue triangles) in agarose gels,[36] and RNAase (red diamonds) and bovine serum albumin (red pentagons) in acrylamide gels.[37]

3.2. Specific-Gel Interacting Counterion Solute. Figure 4 shows fluorescence micrographs and transient concentration profiles (solid lines) for Fl-avidin loaded into and released from a 70 wt % HEMA/30 wt % MAA hydrogel with 0.05 wt % cross-link density. Loading is far from complete after 6 days compared to at most 3 days for full saturation by dextran solutes of similar size. Desorption was initiated at 6 days and continued for 16 days.

The release profile in Figure 4b reveals both farther solute penetration into the gel compared to the loading profile and back extraction into the bulk aqueous solution. After 2 weeks of leaching, however, only 20% of the initially loaded solute is released into the surroundings. Application of Fick's law in eq 1 to predict loading profiles gives an average absorption diffusion coefficient of 7.2×10^{-10} cm²/s for several repeat runs. This diffusion coefficient is 3 orders of magnitude smaller than those for the dextran solutes in Table 3. Apparently, absorption is slowed not only by molecular diffusion, but also by specific attraction of Fl-avidin to the gel matrix.

4. COMPARISON TO THEORY

4.1. Nonspecific-Interacting Solutes. Numerous theories are available to quantify solute diffusion when specific interaction with the gel is negligible.[9,32−38,40−42,45] Most all, including free-volume theory,[42,45] however, require empirical adjustable parameters, and do not make use of measured gel mesh size or gel fiber radius. Table 5 displays three current physical-based theories that allow a priori prediction of hindered solute diffusion in hydrogels. All follow the suggestion of Brady[41] and express the relative diffusivity as a product of a hydrodynamic-resistance factor, F, and a steric or obstruction factor, S, related inversely to tortuosity or
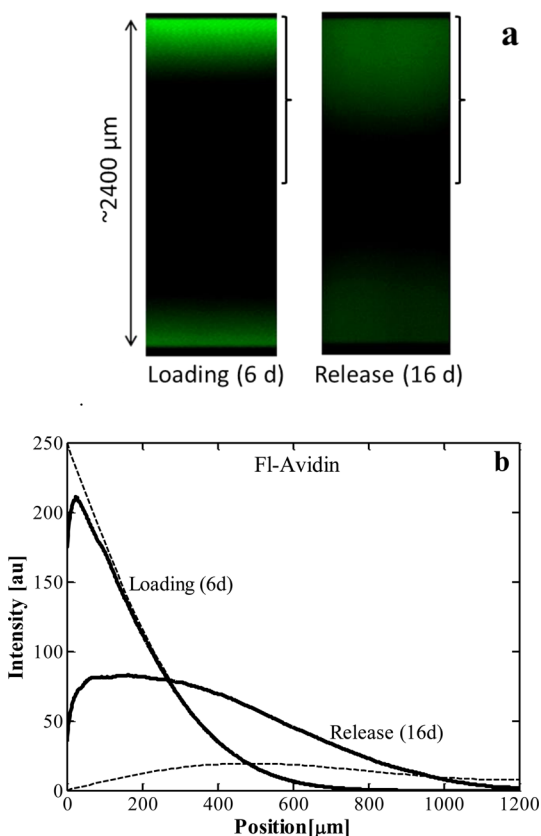
$$D/D_o = FS \tag{5}$$

Figure 4. (a) Fluorescence micrographs and (b) transient intensity profiles (solid lines) of Fl-avidin (0.12 mg/mL solution) in 70 wt % HEMA/30 wt % MAA gel with 0.05 wt % cross-link density. $a_S = 7.1$ nm; $\langle \xi \rangle = 8.3$ nm. Loading for 6 days followed by release for 16 days. Profiles correspond to the top half of the gel (denoted by brackets in (a)). Dashed lines are predicted from eqs 3 and 4 for loading and release, respectively, with a diffusion coefficient of 7.2×10^{-10} cm^2/s best fit from the loading profile.

where D and D_o are the diffusion coefficients in the hydrogel and bulk solution, respectively.[33,36,37,40,57] In these expressions, $\alpha \equiv \varphi(1 + a_S/a_f)^2$, where a_S is the solute radius and a_f is the gel fiber radius.

Hydrodynamic drag is ignored (i.e., $F = 1$) in the Ogston expression for D/D_o, top row in Table 5. Conversely, Clague and Phillips[49] simulated hydrodynamic drag on a sphere in a random arrangement of cylindrical fibers giving $F = \exp(-a\phi^b)$ with a and b established from the simulations. To account for obstruction, Philips[33] adopted the stochastic simulations of Johansson and Löfroth[50] represented by $S = \exp(-0.84\alpha^{1.09})$. In Brinkman effective-medium theory,[71,72] bottom row in Table 5, hydrodynamic drag is given by

$$F = \left[1 + (a_S/\sqrt{\kappa}) + \frac{1}{9}(a_S/\sqrt{\kappa})^2 \right]^{-1} \quad (6)$$

where κ is the absolute hydrodynamic (Darcy) permeability of aqueous solvent in the gel. The accompanying steric factor in Table 5 originates from the analytical cylindrical-cell theory of Johansson et al.[34] that well represents the hard-sphere steric simulations of Johansson and Löfroth.[50]

To implement the Brinkman effective-medium theory, we invoke the Carman–Kozeny expression for hydrodynamic permeability: $\kappa = (1 - \varphi)\langle r_H^2 \rangle/2\tau_H^2$, where $\langle r_H^2 \rangle$ is the mean square hydraulic radius and τ_H is the gel hydrodynamic tortuosity.[32,60] For a random array of fibers with negligible overlap,[30] the mean hydraulic radius is $a_f(1 - \varphi)/2\varphi$, revealing that κ scales as the square of the polymer-strand radius with the familiar Carman–Kozeny porosity dependence

$$\kappa = \frac{(1 - \varphi)^3}{8\varphi^2 \tau_H^2} a_f^2 \quad (7)$$

Tortuosity is included in eq 7 to account for increased path length, for channel shape, and for error in employing a hydraulic radius in creeping flow and in approximating the mean-square hydraulic radius by the square mean. To establish τ_H, Figure 5 displays measured hydrodynamic permeability for gels similar to our HEMA/MAA copolymer[73–75] as a function of $(1 - \varphi)^3/\varphi^2$ on logarithmic scales. Hydraulic permeabilities of the hydrogels are extremely low, in the nanodarcy range, due to the molecular size of the polymer strands and to the relatively low water contents of the gels (i.e., due to the small mesh sizes). The unity-slope solid line in Figure 5 is best fit to eq 7. With a_f fixed at 2 nm, we establish a tortuosity of $\tau_H \sim 4.7$ for our HEMA/MAA gels.

Figures 6–8 compare the a priori theories listed in Table 5 to our measured dextran solute diffusivities in the 70 wt % HEMA/30 wt % MAA gels as a function of polymer volume fraction. Obstruction alone in Ogston's model[35] (small dashed lines) significantly overpredicts the data. The combined theory of Phillips[33] (long dashed lines) also does not reduce diffusivity enough, especially for the smaller dextrans. Effective-medium theory (dashed–dotted lines) best represents the data, but careful examination demonstrates a larger solute-size dependence than that from experiment especially for the largest solute. Although the range of polymer volume fractions is limited in Figures 3 and 6–8 (i.e., a narrow range of cross-link densities) and data are scattered, the measured solute-size dependence of D/D_o is weaker than that predicted by all three theories. No simple scaling factor overcomes this disagreement.

A likely explanation for both minimal penetration and faster measured diffusion rates of solutes with sizes larger than the

Table 5. Selected Gel-Diffusion Models

model type	expression[a]	ref
steric	$\dfrac{D}{D_o} = \exp(-\sqrt{\alpha})$	Ogston et al.[35]
hydrodynamic and steric; computational	$\dfrac{D}{D_o} = \exp(-a\phi^b) \exp(-0.84\alpha^{1.09})$	Phillips,[33] Clague and Phillips,[49] Johansson and Löfroth[50]
hydrodynamic and steric; Brinkman effective medium	$\dfrac{D}{D_o} = \left[1 + (a_S/\sqrt{\kappa}) + \dfrac{1}{9}(a_S/\sqrt{\kappa})^2 \right]^{-1} [e^{-\alpha} + \alpha^2 e^{\alpha} E_1(2\alpha)]$	Solomentsev and Anderson,[72] Johansson et al.[34]

[a]$\alpha \equiv \varphi(1 + a_S/a_f)^2$; $a = 3.727 - 2.460(a_f/a_S) + 0.822(a_f/a_S)^2$; $b = 0.358 + 0.366(a_f/a_S) - 0.0939(a_f/a_S)^2$; $E_1(x) = \int_x^\infty (e^{-u}/u) \, du$.
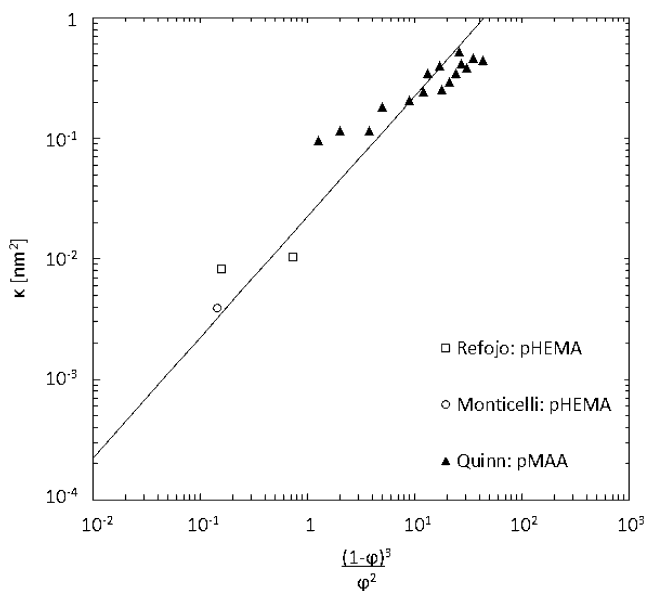
Figure 5. Hydrodynamic permeability, κ, as a function of polymer content expressed as $(1 - \varphi)^3/\varphi^2$ for hydrogels similar to 70 wt % HEMA/30 wt % MAA: Refojo[75] ($\square$); Quinn and Grodzinsky[74] ($\blacktriangle$); Monticelli et al.[73] ($\bigcirc$). With $a_f = 2$ nm, the best-fit unity-slope straight line gives a hydrodynamic tortuosity of $\tau_H = 4.7$.
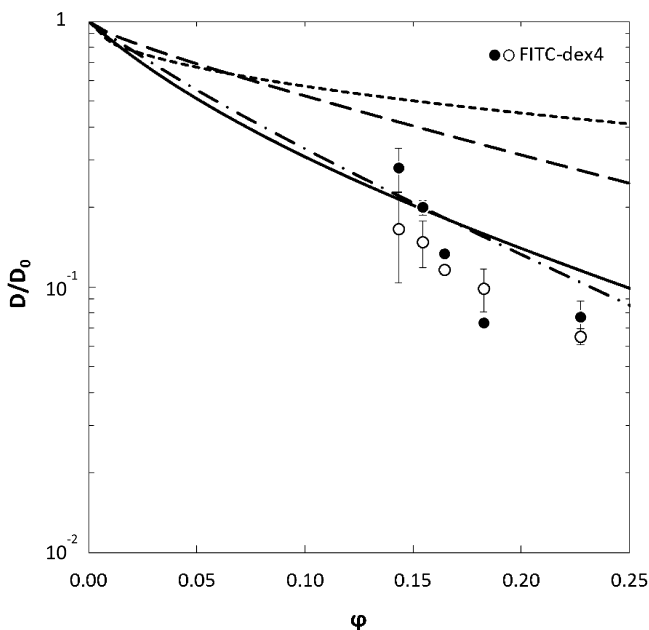

Figure 6. Relative diffusion coefficients of FITC-dextran4 ($\bullet$, $\bigcirc$) in 70 wt % HEMA/30 wt % MAA hydrogels as a function of polymer volume fraction. Filled symbols correspond to the loading direction, while open symbols correspond to the release direction. Lines reflect the predictions of Ogston et al.[35] (---), Phillips[33] ($--$), effective-medium theory[34,72] ($-\cdot-$), and LPEM theory (—).

Figure 7. Relative diffusion coefficients FITC-dextran10 ($\blacksquare$, $\square$) in 70 wt % HEMA/30 wt % MAA hydrogels as a function of polymer volume fraction. Filled symbols correspond to the loading direction, while open symbols correspond to the release direction. Lines reflect the predictions of Ogston et al.[35] (---), Phillips[33] ($--$), effective-medium theory[34,72] ($-\cdot-$), and LPEM theory (—).

Figure 8. Relative diffusion coefficients of FITC-dextran20 ($\blacktriangle$, $\triangle$) in 70 wt % HEMA/30 wt % MAA hydrogels as a function of polymer volume fraction. Filled symbols correspond to the loading direction, while open symbols correspond to the release direction. Lines reflect the predictions of Ogston et al.[35] (---), Phillips[33] ($--$), effective-medium theory[34,72] ($-\cdot-$), and LPEM theory (—).

average gel mesh size is that only a fraction of the liquid-filled voids are solute occupied. Hydrogels clearly exhibit a distribution of mesh sizes. Large solutes in high-polymer-content gels penetrate and permeate through the larger interconnected mesh-size spaces.[31] This framework successfully predicts measured equilibrium partition coefficients of the labeled dextrans in our HEMA/MAA gels.[31] The larger is the solute, the larger are the mesh sizes necessary to permit
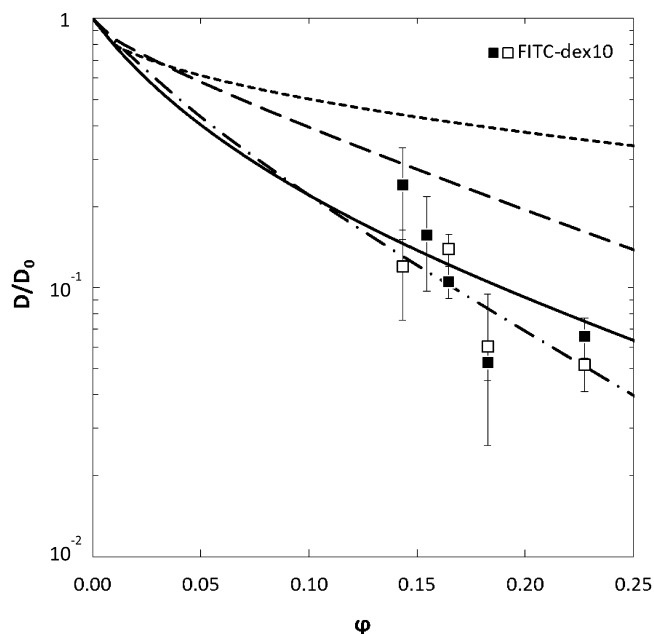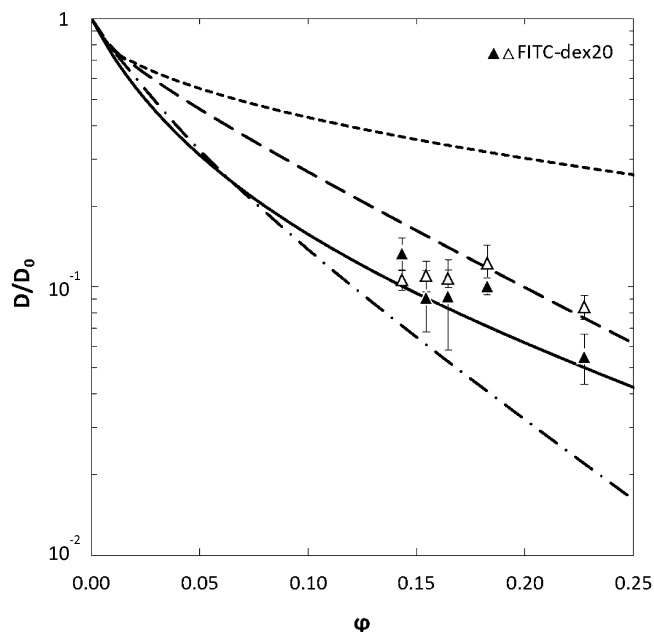
diffusion and the smaller is the fraction of liquid-filled space available for transport.

Current estimates of F and S in Table 5 apply to solutes that are small relative to the gel mesh sizes and do not account for solute-size exclusion from the smaller liquid-filled spaces. Apparently, small solutes experience relatively more hydro-

dynamic drag and obstruction compared to larger ones because of transport through the larger mesh-size spaces. This effect partially offsets the larger drag and obstruction attributed to solute size in current effective-medium theory.

4.2. Large-Pore Effective-Medium Theory. To account for solute transport only in the occupied portion of the gel voids, we create a hypothetical large-pore effective medium (LPEM) consisting of the distribution of mesh sizes available for solute transport. Hydrodynamic and obstruction factors, F[71,72] and S,[34] are modified to describe solute access only to mesh sizes larger than their size and, thus, to account for drag and obstruction only within accessible liquid-filled voids. All liquid-filled pores sizes in the LPEM are assumed to percolate.

The hydrodynamic factor of the large-pore gel is estimated from eqs 6 and 7 but at a larger liquid volume fraction, $1 - \varphi_L$, characteristic of the LPEM. To determine φ_L, we assume that the average hydraulic radius in the large-pore medium, $\langle r_H \rangle_L$, relative to that of the original medium from Carman−Kozeny, i.e., $a_f(1 - \varphi)/2\varphi$, scales linearly with the average mesh radius

$$\langle r_H \rangle_L = [a_f(1 - \varphi)/2\varphi]\langle r \rangle_L/\langle r \rangle \tag{8}$$

where r is the mesh radius or half of the mesh size and subscript "L" indicates the large-pore pseudomedium. The average mesh radius is obtained from the Ogston distribution.[30]

$$a_f g_o(r) = 2\varphi(1 + r/a_f) \exp[-\varphi(1 + r/a_f)^2] \tag{9}$$

where $g_o(r;a_f)$ dr is the volume fraction of water-filled spaces with radii between r and $r + dr$. The average mesh radius of the original distribution and that of the LPEM follow by definition

$$\langle r \rangle = \frac{\int_0^\infty r g_o(r)\, dr}{\int_0^\infty g_o(r)\, dr} = \frac{a_f}{2}\sqrt{\frac{\pi}{\varphi}}\, \exp(\varphi)\, \mathrm{erfc}(\sqrt{\varphi}) \tag{10}$$

and

$$\langle r \rangle_L = \frac{\int_{a_S}^\infty r g_o(r)\, dr}{\int_{a_S}^\infty g_o(r)\, dr}$$
$$= a_S + \frac{a_f}{2}\sqrt{\frac{\pi}{\varphi}} \times \exp(\varphi(1 + a_S/a_f)^2)$$
$$\times \mathrm{erfc}[\sqrt{\varphi}(1 + a_S/a_f)] \tag{11}$$

respectively. Equations 8−11 give the polymer fraction of the LPEM since $\langle r_H \rangle_L \equiv a_f(1 - \varphi_L)/2\varphi_L$. Darcy permeability of the accessible voids, κ_L, is then available from eq 7 with φ replaced by φ_L. The hydrodynamic factor follows from eq 6. We do not adjust the hydraulic tortuosity of the LPEM in eq 7.

The LPEM-modified obstruction factor emerges from two extensions of the cylindrical-cell model of Johansson et al.[34] First, we correct the original expression of Johansson et al.[34] for the diffusion coefficient, $D(R)$, of solute transporting across a single cylindrical cell of radius R[76,77] to read

$$\frac{D(R)}{D_o} = \frac{1 - a^2/R^2}{1 + a^2/R^2} \tag{12}$$

where $a = a_S + a_f$. Adoption of eq 12 gives a slightly modified expression for the obstruction factor: $S = (1 - \alpha)e^{-\alpha} + 2\alpha^2 e^\alpha E_1(2\alpha)$, where $\alpha \equiv \varphi(1 + a_S/a_f)^2$ and E_1 is the exponential integral, $E_1(x) = \int_x^\infty (e^{-u}/u)\, du$. Second, we replace the original-medium polymer volume fraction by that of the hypothetical large-pore medium

$$S = (1 - \alpha_L)e^{-\alpha_L} + 2\alpha_L^2 e^{\alpha_L} E_1(2\alpha_L) \tag{13}$$

where $\alpha_L = \varphi_L(1 + a_S/a_f)^2$. Equation 13 explicitly accounts for occupancy of solute only in the large liquid-filled voids and for excluded volume within those larger pores. The LPEM-modified obstruction factor also agrees with the hard-sphere steric simulations of Johansson and Loforoth.[50] With F and S now specified in eqs 6 and 13, solute diffusivity in the gel follows from eq 5.

Solid lines in Figures 6−8 display predictions of the proposed LPEM theory for the relative diffusivities of FITC-dextran4, FITC-dextran10, and FITC-dextran20 in the 70 wt % HEMA/30 wt % MAA gels measured as a function of polymer volume fraction using no adjustable parameters. Agreement for all noninteracting solutes is acceptable to within, at most, a factor of 2. Thus, LPEM theory well predicts diffusion coefficients of large solutes (relative to mesh size) in high polymer content gels with no adjustable constants.

4.3. Specific-Interacting Counterion Solute. The slow loading and release of cationic Fl-avidin shown in Figure 4 coupled with the large measured partition coefficient of 23.9[31] and the small loading diffusion coefficient of 7.2×10^{-10} cm^2/s indicates strong specific adsorption to the HEMA/MAA polymer chains. To understand the transport kinetics, we first extend eq 1 to account for the amount of protein specifically adsorbed to the polymer as distinct from that occupying the liquid-filled spaces

$$\frac{\partial C(t, x)}{\partial t} + \left(\frac{\varphi}{1 - \varphi}\right)\frac{\partial n(t, x)}{\partial t} = D\frac{\partial^2 C(t, x)}{\partial x^2} \tag{14}$$

where C is the moles of nonadsorbed solute in the liquid-filled voids per liquid volume and n is the moles of specifically adsorbed solute per unit polymer volume in the gel.[31] Equation 14 assumes that the dilute solute does not influence swelling, that diffusion occurs only in the liquid phase of the gel, and that surface diffusion along the polymer backbone is negligible. This approach contrasts with that of Russell et al.,[29] who make no distinction between liquid-phase and chain-surface transport in a gel.

To describe the rate of adsorption, the simplest approach is to assume local equilibrium with a linear isotherm: $n = KC$, where K is Henry's adsorption constant (dimensionless).[31] Substitution of Henry's law into eq 14 yields an effective diffusion coefficient governing transport in the gel: $D_e = D/[1 + \varphi K/(1 - \varphi)]$. Accordingly, specific adsorption of solute onto the polymer chains with a large Henry's constant drastically retards diffusion rates. The measured Henry's adsorption constant for Fl-avidin is 5500,[31] giving an effective diffusion coefficient 3 orders of magnitude smaller than that for a nonadsorbing solute of the same size, qualitatively consistent with the observed loading diffusion coefficient of Fl-avidin. Quantitative agreement between the calculated D_e and the measured loading diffusion coefficient from Figure 4b, however, is lacking.

The lower dashed line in Figure 4b reflects the predicted release profile after $t^* = 16$ days of leaching using eq 2, the expression $C(t,x)/C_\infty = \sum_{n=0}^\infty A_n(t,x;t^*)$ and the measured loading diffusion coefficient of 7.2×10^{-10} cm^2/s. Because the amount of solute adsorbed is linearly proportional to the liquid-phase concentration, separate accounting for $n(t,x)$ is not requisite. In Figure 4b, theory predicts that 75% of the initially

loaded solute is released over the 16-day extraction period, much more than the measured 20%.

The large discrepancy between observed and predicted Fl-avidin release kinetics in Figure 4b and the quantitative disagreement between calculated and measured D_e values suggest that local sorption equilibrium is not attained within the gel. To relieve the local-equilibrium restriction, we invoke simple linear adsorption/desorption kinetics for the solute in the gel

$$\frac{\partial n(t, x)}{\partial t} = k_{-1}[KC - n] \tag{15}$$

so that

$$\frac{\partial C(t, x)}{\partial t} = D\frac{\partial^2 C(t, x)}{\partial x^2} - \left(\frac{\varphi}{1 - \varphi}\right)k_{-1}[KC - n] \tag{16}$$

where k_{-1} is the first-order desorption rate constant and $k_{-1}K$ is the first-order adsorption rate constant. The solution to eqs 15 and 16 is given in the Appendix. As with loading of the nonadsorbing solutes because of surface blotting, we first estimate the surface concentration $C(t, -L) = C_\infty$ in eq A3 from the Fl-avidin loading profile in Figure 4b near the top face of the gel. The remainder of the loading profile at 6 days is then fit to obtain the desorption rate constant and the diffusion coefficient of Fl-avidin in the 70 wt % HEMA/30 wt % MAA gel.

The upper dashed line in Figure 9 shows the resulting model fit to the measured loading profile with $D/D_o = 0.5$ and $k_{-1} = 6$
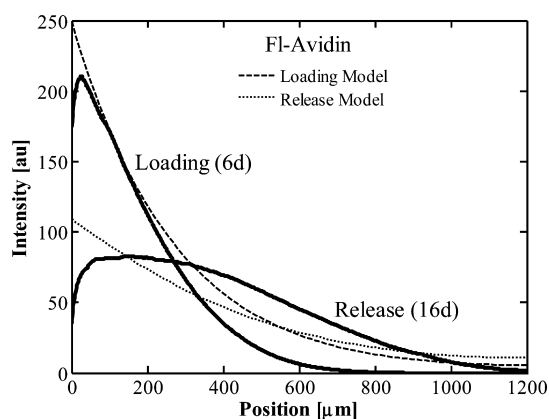

Figure 9. Transient loading and release profiles (bold lines) of Fl-avidin in a 70 wt % HEMA/30 wt % MAA hydrogel with 0.05 wt % cross-link density. Desorption begins after 6 days of loading. Dashed and dotted lines are predicted from linear sorption kinetics with $D/D_o = 0.5$, $K = 5500$, and $k_{-1} = 6 \times 10^{-7}$ s^{-1}.

$\times 10^{-7}$ s^{-1} giving a characteristic desorption time of 19 days. Shown in the lower dotted line is the corresponding release profile of Fl-avidin predicted with no adjustable parameters. Although not quantitative, agreement of the measured profiles with the linear-kinetic model is much improved over that based on the local-equilibrium assumption shown in Figure 4b. The observed small desorption rate constant suggests that Fl-avidin is tightly bound to the polymer strands, approaching irreversible attachment, typical for proteins at long exposure times.[78−82] Strict conformance to linear sorption kinetics is, therefore, unlikely. Additional transient-profile data at differing Fl-avidin concentrations are necessary to establish more realistic sorption kinetics.

Considerable size exclusion is expected for the 7.1-nm avidin molecule in the 8.3-nm mesh-size gel. Accordingly, Fl-avidin penetrates only a small fraction of the aqueous-occupied voids.[31] In view of the small voidage occupancy, the large measured Henry's adsorption constant and the concomitant small desorption rate constant indicate strong specific adsorption on the polymer matrix. Donnan electrostatic attraction[83] is an unlikely explanation because of extensive screening by the background aqueous electrolyte at a Debye length of 0.5 nm. Rather, the experimental evidence strongly supports specific ion binding between cationic Fl-avidin and anionic MAA groups along the polymer strands.

5. CONCLUSIONS

Using two-photon confocal fluorescence microscopy, we measured transient loading and release concentration profiles of four labeled aqueous solutes: FITC-dextrans of 4, 10, and 20 kDa molecular weights, and fluorescein conjugate avidin, at pH 7.4, in negatively charged 70 wt % HEMA/30 wt % MAA hydrogels having 0−1 wt % cross-link density. A unique feature of our measurements is that solute size is comparable to or larger than the average mesh size of the gels and the polymer volume fraction range is higher than those typically studied. Although all solutes are significantly size-excluded from major portions of the gel voids, they all permeate through the available gel network by liquid-phase diffusion. Except for cationic Fl-avidin, all solutes exhibit reversible absorption and desorption with diffusion coefficients approximately equal in both directions in obedience to Fick's second law. For these nonadsorbing solutes, gel diffusivities decrease strongly with increasing polymer content and less so with increasing solute size. LPEM theory gives D/D_o as a product of a hydrodynamic factor, F, and an obstruction factor, S, taking into account only gel mesh sizes available for transport. When all parameters are independently determined, LPEM theory agrees quantitatively with measured solute diffusion coefficients. Accordingly, an estimate of nonadsorbing aqueous-solute transport rates in hydrogels is available without the need to adjust parameters. Although LPEM is physically grounded, it does not account for dynamic fluctuations in the mesh-size distribution.

For the positively charged counterion Fl-avidin solute, diffusion is significantly slowed by strong specific adsorption on the anionic polymer strands. When compared to a dextran molecule of the same hydrodynamic size, avidin absorbs more slowly into the gel by over 3 orders of magnitude. Desorption is even slower, approaching irreversible uptake. An effective local-equilibrium diffusion coefficient does not predict uptake and release kinetics. Simple linear adsorption/desorption kinetics more successfully fits the measured concentration profiles, giving a desorption time constant of about 20 days. The large measured Henry's adsorption constant and the small desorption rate constant highlight strong ion binding of the cationic avidin onto the anionic MAA moieties of the gel polymer. The difference between diffusion rates of non-adsorbing and specific adsorbing solutes in hydrogels is striking and must be accounted for.

■ APPENDIX: SOLUTION TO LINEAR-ADSORPTION KINETICS MODEL

Boundary conditions for eqs 14 and 15 are described in section 4.3 for loading and release after a time t^*. Convenient solution of these equations is by Laplace transform with inversion by

residues and convolution.[84] The measured concentration per unit volume of gel is the sum of that in the liquid pores and that on the gel strands: $C_m = (1 - \varphi)C + \varphi n$. Let $B_n(x;t^*)$ be defined as

$$
B_n(x; t^*) \equiv 2\frac{(-1)^n}{\lambda_n} \frac{(1 + S_n)}{S_n[1 + \Phi^2(1 + rK + 2S_n)/\lambda_n^2]}
$$
$$
\times \cos[\lambda_n x/L]\{\exp[S_n k_{-1} t^*] - 1\} \tag{A1}
$$

where $\lambda_n \equiv (2n + 1)\pi/2$, $r \equiv \varphi/(1 - \varphi)$, $\Phi^2 \equiv k_{-1}L^2/D$ is the Thiele parameter, and

$$
2S_n\Phi^2\lambda_n^{-2} = -[1 + (1 + rK)\Phi^2/\lambda_n^2]
$$
$$
\pm \sqrt{[1 + (1 + rK)\Phi^2/\lambda_n^2]^2 - 4\Phi^2/\lambda_n^2} \tag{A2}
$$

Accordingly, for loading into a gel initially devoid of solute, the measured concentration profile obeys the expression

$$
\frac{C_m(t, x; \infty)}{(1 - \varphi)C_\infty} = 1 - \sum_{n=0}^{\infty} B_n(x; \infty) \exp[S_n k_{-1} t]
$$
$$
+ rK\Bigg[1 - \exp[-k_{-1}t]
$$
$$
- \sum_{n=0}^{\infty} (1 + S_n)^{-1} B_n(x; \infty)
$$
$$
\times \{\exp[S_n k_{-1} t] - \exp[-k_{-1}t]\}\Bigg] \tag{A3}
$$

The first two terms on the right of eq A3 correspond to the solute concentration in the liquid-filled voids per unit gel volume, while the last term on the right corresponds to solute adsorbed on the polymer matrix per unit gel volume. Because adsorption is not instantaneous, the amount adsorbed at $x = -L$ rises while solute concentration in the gel pores remains at C_∞.

The case of desorption from a partially saturated gel is more complicated. We find for extraction from an initial solute concentration profile at t^* that

$$
\frac{C_m(t, x; t^*)}{(1 - \varphi)C_\infty} = \Bigg[\sum_{n=0}^{\infty} B_n(x; t^*) \exp[S_n k_{-1} t]\Bigg]
$$
$$
+ rK\Bigg[\sum_{n=0}^{\infty} (1 + S_n)^{-1} B_n(x; t^*) \times \{\exp[S_n k_{-1} t]
$$
$$
- \exp[-k_{-1}t]\}\Bigg] + rK \exp[-k_{-1}t]\Bigg[1 - \exp[-k_{-1}t^*]
$$
$$
- \sum_{n=0}^{\infty} (1 + S_n)^{-1} B_n(x; \infty)
$$
$$
\times \{\exp[S_n k_{-1} t^*] - \exp[-k_{-1}t^*]\}\Bigg] \tag{A4}
$$

Again, the first term on the right of eq A4 reflects the solute profile in the liquid-filled voids of the gel, while the second two terms on the right correspond to the adsorption profile. Factors in which t^* appears reflect the initial partially saturated solute

profile. Both roots in eq A2 are used as are over 100 terms in the indicated summations.

■ AUTHOR INFORMATION

Corresponding Author
*E-mail: radke@berkeley.edu. Tel.: (510) 642-5204. Fax: (510) 642-4778.

Notes
The authors declare no competing financial interest.

■ REFERENCES

(1) Boschetti, E. Advanced sorbents for preparative protein separation purposes. *J. Chromatogr., A* **1994**, 658, 207−236.

(2) Farnan, D.; Frey, D. D.; Horváth, C. Surface and pore diffusion in macroporous and gel-filled gigaporous stationary phases for protein chromatography. *J. Chromatogr., A* **2002**, 959, 65−73.

(3) Fernandez, M. A.; Carta, G. Characterization of protein adsorption by composite silica-polyacrylamide gel anion exchangers I. Equilibrium and mass transfer in agitated contactors. *J. Chromatogr., A* **1996**, 746, 169−183.

(4) Farnan, D.; Frey, D. D.; Horvath, C. Intraparticle mass transfer in high-speed chromatography of proteins. *Biotechnol. Prog.* **1997**, 13, 429−439.

(5) Peppas, N. A.; Bures, P.; Leobandung, W.; Ichikawa, H. Hydrogels in pharmaceutical formulations. *Eur. J. Pharm. Biopharm.* **2000**, 50, 27−46.

(6) Jen, A. C.; Wake, M. C.; Mikos, A. G. Review: Hydrogels for cell immobilization. *Biotechnol. Bioeng.* **1996**, 50, 357−364.

(7) Drury, J. L.; Mooney, D. J. Hydrogels for tissue engineering: scaffold design variables and applications. *Biomaterials* **2003**, 24, 4337−4351.

(8) Kretsinger, J. K.; Haines, L. A.; Ozbas, B.; Pochan, D. J.; Schneider, J. P. Cytocompatibility of self-assembled β-hairpin peptide hydrogel surfaces. *Biomaterials* **2005**, 26, 5177−5186.

(9) Amsden, B. Solute diffusion in hydrogels: An examination of the retardation effect. *Polym. Gels Networks* **1998**, 6, 13−43.

(10) Jones, D. S.; Lorimer, C. J.; Andrews, G. P.; McCoy, C. P.; Gorman, S. P. An examination of the thermorheological and drug release properties of zinc tetraphenylporphyrin-containing thermoresponsive hydrogels, designed as light activated antimicrobial implants. *Chem. Eng. Sci.* **2007**, 62, 990−999.

(11) Peppas, N. A.; Langer, R. New challenges in biomaterials. *Science* **1994**, 263, 1715−1720.

(12) Castillo, E. J.; Koenig, J. L.; Anderson, J. M.; Lo, J. Protein adsorption on hydrogels: II. Reversible and irreversible interactions between lysozyme and soft contact lens surfaces. *Biomaterials* **1985**, 6, 338−345.

(13) Luensmann, D.; Zhang, F.; Subbaraman, L.; Sheardown, H.; Jones, L. Localization of lysozyme sorption to conventional and silicone hydrogel contact lenses using confocal microscopy. *Curr. Eye Res.* **2009**, 34, 683−697.

(14) Nicolson, P. C.; Vogt, J. Soft contact lens polymers: an evolution. *Biomaterials* **2001**, 22, 3273−3283.

(15) Alvarez-Lorenzo, C.; Hiratani, H.; Concheiro, A. Contact Lenses for Drug Delivery: Achieving Sustained Release with Novel Systems. *Am. J. Drug Delivery* **2006**, 4, 131−151.

(16) Venkatesh, S.; Sizemore, S. P.; Byrne, M. E. Biomimetic hydrogels for enhanced loading and extended release of ocular therapeutics. *Biomaterials* **2007**, 28, 717−724.

(17) Peng, C.-C.; Kim, J.; Chauhan, A. Extended delivery of hydrophilic drugs from silicone-hydrogel contact lenses containing Vitamin E diffusion barriers. *Biomaterials* **2010**, 31, 4032−4047.

18118

dx.doi.org/10.1021/ie402148u | *Ind. Eng. Chem. Res.* 2013, 52, 18109−18120

(18) Xinming, L.; Yingde, C.; Lloyd, A. W.; Mikhalovsky, S. V.; Sandeman, S. R.; Howel, C. A.; Liewen, L. Polymeric hydrogels for novel contact lens-based ophthalmic drug delivery systems: A review. *Contact Lens Anterior Eye* **2008**, *31*, 57−64.

(19) White, C.; Tieppo, A.; Byrne, M. Controlled drug release from contact lenses: a comprehensive review from 1965-present. *J. Drug Delivery Sci. Technol.* **2011**, *21*, 369−384.

(20) Ketelson, H. A.; Meadows, D. L.; Stone, R. P. Dynamic wettability properties of a soft contact lens hydrogel. *Colloids Surf., B* **2005**, *40*, 1−9.

(21) Tran, V. B.; Sung, Y. S.; Copley, K.; Radke, C. J. Effects of aqueous polymeric surfactants on silicone-hydrogel soft- contact-lens wettability and bacterial adhesion of Pseudomonas aeruginosa. *Contact Lens Anterior Eye* **2012**, *35*, 155−162.

(22) Peppas, N. A.; Moynihan, H. J.; Lucht, L. M. The structure of highly crosslinked poly(2-hydroxyethyl methacrylate) hydrogels. *J. Biomed. Mater. Res.* **1985**, *19*, 397−411.

(23) Anseth, K. S.; Bowman, C. N.; Brannon-Peppas, L. Mechanical properties of hydrogels and their experimental determination. *Biomaterials* **1996**, *17*, 1647−1657.

(24) D'Errico, G.; De Lellis, M.; Mangiapia, G.; Tedeschi, A.; Ortona, O.; Fusco, S.; Borzacchiello, A.; Ambrosio, L. Structural and Mechanical Properties of UV-Photo-Cross-Linked Poly(N-vinyl-2-pyrrolidone) Hydrogels. *Biomacromolecules* **2007**, *9*, 231−240.

(25) De Gennes, P. G. *Scaling Concepts in Polymer Physics*; Cornell University Press: Ithaca, NY, 1979.

(26) Lewus, R. K.; Carta, G. Protein diffusion in charged polyacrylamide gels: visualization and analysis. *J. Chromatogr., A* **1999**, *865*, 155−168.

(27) Lewus, R. K.; Carta, G. Protein transport in constrained anionic hydrogels: diffusion and boundary-layer mass transfer. *Ind. Eng. Chem. Res.* **2001**, *40*, 1548−1558.

(28) Russell, S. M.; Belcher, E. B.; Carta, G. Protein partitioning and transport in supported cationic acrylamide-based hydrogels. *AIChE J.* **2003**, *49*, 1168−1177.

(29) Russell, S. M.; Carta, G. Multicomponent protein adsorption in supported cationic polyacrylamide hydrogels. *AIChE J.* **2005**, *51*, 2469−2480.

(30) Ogston, A. G. The spaces in a uniform random suspension of fibres. *Trans. Faraday Soc.* **1958**, *54*, 1754−1757.

(31) Kotsmar, C.; Sells, T.; Taylor, N.; Liu, D. E.; Prausnitz, J. M.; Radke, C. J. Aqueous solute partitioning and mesh size in HEMA/MAA hydrogels. *Macromolecules* **2012**, *45*, 9177−9187.

(32) Pluen, A.; Netti, P. A.; Jain, R. K.; Berk, D. A. Diffusion of macromolecules in agarose gels: Comparison of linear and globular configurations. *Biophys. J.* **1999**, *77*, 542−552.

(33) Phillips, R. J. A hydrodynamic model for hindered diffusion of proteins and micelles in hydrogels. *Biophys. J.* **2000**, *79*, 3350.

(34) Johansson, L.; Elvingson, C.; Löfroth, J. E. Diffusion and interaction in gels and solutions. 3. Theoretical results on the obstruction effect. *Macromolecules* **1991**, *24*, 6024−6029.

(35) Ogston, A.; Preston, B.; Wells, J. On the transport of compact particles through solutions of chain-polymers. *Proc. R. Soc. London, A: Math. Phys. Sci.* **1973**, *333*, 297−316.

(36) Johnson, E. M.; Berk, D. A.; Jain, R. K.; Deen, W. M. Hindered diffusion in agarose gels: test of effective medium model. *Biophys. J.* **1996**, *70*, 1017−1023.

(37) Tong, J.; Anderson, J. L. Partitioning and diffusion of proteins and linear polymers in polyacrylamide gels. *Biophys. J.* **1996**, *70*, 1505−1513.

(38) Lustig, S. R.; Peppas, N. A. Solute diffusion in swollen membranes. IX. Scaling laws for solute diffusion in gels. *J. Appl. Polym. Sci.* **1988**, *36*, 735−747.

(39) Peppas, N. A.; Reinhart, C. T. Solute diffusion in swollen membranes. Part I. A new theory. *J. Membr. Sci.* **1983**, *15*, 275−287.

(40) Phillips, R. J.; Deen, W. M.; Brady, J. F. Hindered transport in fibrous membranes and gels: Effect of solute size and fiber configuration. *J. Colloid Interface Sci.* **1990**, *139*, 363−373.

(41) Brady, J. Hindered diffusion. In *Extended Abstracts, AIChE Annual Meeting, San Fransisco, CA, 1994*; AIChE: New York, 1994; p 320.

(42) Amsden, B. Solute diffusion within hydrogels. Mechanisms and models. *Macromolecules* **1998**, *31*, 8382−8395.

(43) Grassi, M.; Lapasin, R.; Coviello, T.; Matricardi, P.; Di Meo, C.; Alhaique, F. Scleroglucan/borax/drug hydrogels: Structure characterisation by means of rheological and diffusion experiments. *Carbohydr. Polym.* **2009**, *78*, 377−383.

(44) Waters, D. J.; Frank, C. W. Hindered diffusion of oligosaccharides in high strength poly(ethylene glycol)/poly(acrylic acid) interpenetrating network hydrogels: Hydrodynamic vs. obstruction models. *Polymer* **2009**, *50*, 6331−6339.

(45) Masaro, L.; Zhu, X. X. Physical models of diffusion for polymer solutions, gels and solids. *Prog. Polym. Sci.* **1999**, *24*, 731−775.

(46) Guan, L.; Jiménez, M. E. G.; Walowski, C.; Boushehri, A.; Prausnitz, J. M.; Radke, C. J. Permeability and partition coefficient of aqueous sodium chloride in soft contact lenses. *J. Appl. Polym. Sci.* **2011**, *122*, 1457−1471.

(47) am Ende, M. T.; Peppas, N. A. Transport of ionizable drugs and proteins in crosslinked poly(acrylic acid) and poly(acrylic acid-co-2-hydroxyethyl methacrylate) hydrogels. II. Diffusion and release studies. *J. Controlled Release* **1997**, *48*, 47−56.

(48) Kong, D. D.; Kosar, T. F.; Dungan, S. R.; Phillips, R. J. Diffusion of proteins and nonionic micelles in agarose gels by holographic interferometry. *AIChE J.* **1997**, *43*, 25−32.

(49) Clague, D. S.; Phillips, R. J. Hindered diffusion of spherical macromolecules through dilute fibrous media. *Phys. Fluids* **1996**, *8*, 1720.

(50) Johansson, L.; Löfroth, J. E. Diffusion and interaction in gels and solutions. 4. Hard sphere Brownian dynamics simulations. *J. Chem. Phys.* **1993**, *98*, 7471.

(51) Johnson, E. M.; Berk, D. A.; Jain, R. K.; Deen, W. M. Diffusion and partitioning of proteins in charged agarose gels. *Biophys. J.* **1995**, *68*, 1561−1568.

(52) Amsden, B. An obstruction-scaling model for diffusion in homogeneous hydrogels. *Macromolecules* **1999**, *32*, 874−879.

(53) Bosma, J.; Wesselingh, J. Partitioning and diffusion of large molecules in fibrous structures. *J. Chromatogr., B: Biomed. Sci. Appl.* **2000**, *743*, 169−180.

(54) Phillips, R.; Deen, W.; Brady, J. Hindered transport of spherical macromolecules in fibrous membranes and gels. *AIChE J.* **1989**, *35*, 1761−1769.

(55) Lazzara, M. J.; Blankschtein, D.; Deen, W. M. Effects of multisolute steric interactions on membrane partition coefficients. *J. Colloid Interface Sci.* **2000**, *226*, 112−122.

(56) Shalviri, A.; Liu, Q.; Abdekhodaie, M. J.; Wu, X. Y. Novel modified starch−xanthan gum hydrogels for controlled drug delivery: Synthesis and characterization. *Carbohydr. Polym.* **2010**, *79*, 898−907.

(57) Fatin-Rouge, N.; Wilkinson, K. J.; Buffle, J. Combining small angle neutron scattering (SANS) and fluorescence correlation spectroscopy (FCS) measurements to relate diffusion in agarose gels to structure. *J. Phys. Chem. B* **2006**, *110*, 20133−20142.

(58) Newman, J.; Chapman, T. W. Restricted diffusion in binary solutions. *AIChE J.* **1973**, *19*, 343−348.

(59) Stewart, S. G.; Newman, J. The use of UV/vis absorption to measure diffusion coefficients in LiPF6 electrolytic solutions. *J. Electrochem. Soc.* **2008**, *155*, F13−F16.

(60) Bird, R. B.; Stewart, W. E.; Lightfoot, E. N. *Transport Phenomena*; Wiley: New York, 2006.

(61) Kopeček, J.; Lím, D. Mechanism of the three-dimensional polymerization of glycol methacrylates. II. The system glycol monomethacrylate−glycol dimethacrylates−solvents. *J. Polym. Sci., Part A-1: Polym. Chem.* **1971**, *9,*, 147−154.

(62) Erman, B.; Mark, J. E. *Structures and Properties of Rubberlike Networks*; Oxford University Press: New York, 1997.

(63) Hasa, J.; Ilavský, M. Deformational, swelling, and potentiometric behavior of ionized poly(methacrylic acid) gels. II. Experimental results. *J. Polym. Sci.: Polym. Phys. Ed.* **1975**, *13*, 263−274.

(64) Göppert-Mayer, M. Über elementarakte mit zwei quanten-sprüngen. *Ann. Phys.* **1931**, *401*, 273−294.

(65) Denk, W.; Strickler, J. P.; Webb, W. W. Two-Photon Laser Microscopy. U.S. Patent 5,034,613, 1991.

(66) Song, Y.; Srinivasarao, M.; Tonelli, A.; Balik, C.; McGregor, R. Laser scanning confocal microscopy study of dye diffusion in fibers. *Macromolecules* **2000**, *33*, 4478−4485.

(67) Michielsen, S. Aberrations in confocal spectroscopy of polymeric materials: erroneous thicknesses and intensities, and loss of resolution. *J. Appl. Polym. Sci.* **2001**, *81*, 1662−1669.

(68) Russell, S. M.; Carta, G. Mesh size of charged polyacrylamide hydrogels from partitioning measurements. *Ind. Eng. Chem. Res.* **2005**, *44*, 8213−8217.

(69) Origin Pro, version 8 (8.0724); OriginLab; 2012. http://www.originlab.com/index.aspx?go=Products/Origin/DataAnalysis/SignalProcessing/SmoothingAndFitting&pid=62.

(70) Press, W. H.; Teukolsky, S. A.; Vetterling, W. T.; Flannery, B. P. *Numerical Recipes*; Cambridge University Press: Cambridge, U.K., 1992.

(71) Brinkman, H. C. A calculation of the viscous force exerted by a flowing fluid on a dense swarm of particles. *Appl. Sci. Res.* **1949**, *1*, 27−34.

(72) Solomentsev, Y. E.; Anderson, J. L. Rotation of a sphere in Brinkman fluids. *Phys. Fluids* **1996**, *8*, 1119.

(73) Monticelli, M.; Chauhan, A.; Radke, C. The effect of water hydraulic permeability on the settling of a soft contact lens on the eye. *Curr. Eye Res.* **2005**, *30*, 329−336.

(74) Quinn, T. M.; Grodzinsky, A. J. Longitudinal modulus and hydraulic permeability of poly(methacrylic acid) gels: effects of charge density and solvent content. *Macromolecules* **1993**, *26*, 4332−4338.

(75) Refojo, M. F. Permeation of water through some hydrogels. *J. Appl. Polym. Sci.* **1965**, *9*, 3417−3426.

(76) Belloni, L.; Drifford, M.; Turq, P. Counterion diffusion in polyelectrolyte solutions. *Chem. Phys.* **1984**, *83*, 147−154.

(77) Nilsson, L. G.; Nordenskioeld, L.; Stilbs, P.; Braunlin, W. H. Macroscopic counterion diffusion in solutions of cylindrical polyelectrolytes. *J. Phys. Chem.* **1985**, *89*, 3385−3391.

(78) Kim, J.-H.; Yoon, J.-Y., Protein adsorption on polymer particles. In *Encyclopedia of Surface and Colloid Science*; Soma Sundaran, P., Ed.; Marcel Dekker: New York, 2002; Vol. *4*, pp 4373−4381.

(79) Kim, D. T.; Blanch, H. W.; Radke, C. J. Direct imaging of lysozyme adsorption onto mica by atomic force microscopy. *Langmuir* **2002**, *18*, 5841−5850.

(80) Cascão Pereira, L. G.; Hickel, A.; Radke, C. J.; Blanch, H. W. A kinetic model for enzyme interfacial activity and stability: pa-hydroxynitrile lyase at the diisopropyl ether/water interface. *Biotechnol. Bioeng.* **2002**, *78*, 595−605.

(81) Tie, Y.; Calonder, C.; Van Tassel, P. R. Protein adsorption: kinetics and history dependence. *J. Colloid Interface Sci.* **2003**, *268*, 1−11.

(82) Karlsson, M.; Ekeroth, J.; Elwing, H.; Carlsson, U. Reduction of irreversible protein adsorption on solid surfaces by protein engineering for increased stability. *J. Biol. Chem.* **2005**, *280*, 25558−25564.

(83) Overbeek, J. T. G. Electrochemistry of the Double Layer. In *Colloid Science. I. Irreversible Systems*; Kruyt, H. R., Ed.; Elsevier: Amsterdam, 1952.

(84) Carslaw, H. S.; Jaeger, J. C. *Conduction of Heat in Solids*; Oxford University Press: Oxford, U.K., 1959.